

# Nonlinear Control Design for a High-Precision Contactless Positioning System Using Magnetic Levitation

Robert Brydon Owen, Manfredi Maggiore and Jacob Apkarian

**Abstract**—This paper presents the implementation of a two degree-of-freedom, high-precision, magnetic-levitation-based positioning system. The apparatus employs one permanent magnet linear synchronous motor and is constructed by Quanser Inc. The paper focuses on the design and testing of a nonlinear controller required for actuating the positioning system. The controller is based on feedback linearization and output regulation. Experimental results show that the controller is capable of performing both set-point stabilization and sinusoidal tracking over the complete operating range to within a specified degree of accuracy, with an acceptable amount of overshoot and settling time.

## I. INTRODUCTION

In semiconductor manufacturing, many of the process stages require positioning systems, referred to as *microsteppers*, capable of several degrees of freedom (DOF) with significant speed and precision [1]. As new technology causes the dimensions of semiconductors to further decrease, there is an increasing interest to replace traditional mechanical microsteppers by contactless positioning devices, as mechanical actuators introduce impurities into processing and require costly maintenance. Contactless positioning can also be applied in other areas (such as nanotechnology, probing and inspection systems) where significant speed and precision are required at multiple degrees of freedom, and provides challenging nonlinear dynamics for the testing of control theory.

In [2], Kim and Trumper proposed a contactless microstepper in which employs single sided *air cored* permanent magnet linear synchronous motors (PMLSM) to actuate six degrees-of-freedom. Individually, PMLSMs produce both a normal and translational force when sufficient control is applied. When several are combined in appropriate fashion, multiple degrees of freedom can be achieved.

In [3], modelling and nonlinear control designs were presented for an idealized three degrees-of-freedom device which employed *iron cored* PMLSMs. This device was designed to work over a large range of operation and to employ standard PMLSMs commonly found on the market.

This work was supported by the Natural Sciences and Engineering Research Council of Canada (NSERC) and the Canada Foundation for Innovation (CFI). Robert Brydon Owen was partially supported by the Canadian Space Agency

Robert Brydon Owen and Manfredi Maggiore are with the Edward S. Rogers Department of Electrical and Computer Engineering, University of Toronto, 10 King's College Road, Toronto, ON M5S 3G4, Canada. Jacob Apkarian is with Quanser Inc., 80 Esna Park Drive #1, Markham, ON L3R 2R6, Canada. [bowen@control.toronto.edu](mailto:bowen@control.toronto.edu) [maggiore@control.toronto.edu](mailto:maggiore@control.toronto.edu) [jacob.apkarian@quanser.com](mailto:jacob.apkarian@quanser.com)

In [4], two of the authors of this paper initiated the experimental verification of [3], using a simplified 2-DOF apparatus. Specifically, a parameter identification technique developed in [5] was used to estimate the parameters of the model in [3] and then compared the forces predicted by the model to the actual forces exerted by the PMLSM. The comparisons demonstrated the accuracy of the mathematical model over a wide range of operation (100 mm  $\times$  10 mm).

The focus of this paper is to apply the results from [4] in the design of a nonlinear controller capable of set-point stabilization and sinusoidal tracking across the complete operating range of the 2-DOF apparatus, using feedback linearization and output regulation. The goal is to obtain a steady-state set-point accuracy greater than 0.1 mm and an average tracking error approaching 0.1 mm. Because the 2-DOF apparatus is a first generation proof of concept, no other performance specifications were imposed upon the controller.

We begin our discussion with a description of the 2-DOF contactless positioning hardware, along with the corresponding model derivation. This is followed by a brief summary of the system identification and model verification from [4]. The nonlinear controller design procedure is then outlined in conjunction with a series of experimental results. The paper concludes with a description of future extensions to the magnetic levitation implementation.

## II. DESCRIPTION OF 2-DOF HARDWARE

A photo of the hardware implementation is shown in Figure 1. As mentioned earlier, we employ a single sided iron-cored PMLSM. The *stator* of the PMLSM, which is



Fig. 1. 2-DOF magnetic levitation hardware implementation

fixed in place to a heavy aluminium frame, is longitudinally laminated and transversally slotted in order to accommodate a single layer of 3-phase winding. The *mover*, which is

TABLE I  
SPECIFICATIONS FOR 2-DOF MAGNETIC LEVITATION HARDWARE

Parameter	Symbol	units	value
Stator slot width	$b_0$	mm	12.7
Stator slot pitch	$t_1$	mm	19.05
Turns per phase	$W$	–	900
Coil pitch	$\omega_c$	mm	57.15
Stator pole pairs	$p$	–	3
Number of stator slots	$z_1$	–	18
PM height	$h_m$	mm	5
PM length	$L_A$	mm	50
Number of PM's	$p_m$	–	4
Pole pitch	$\tau$	mm	57.15
PM width	$\tau_p$	mm	28.58
PM coercivity	$H_c$	A/m	875400
Back iron height	$h_b$	mm	4.7
Back iron width	–	mm	50
Back iron length	–	mm	200.0
Horizontal Mover Mass	$M_h$	Kg	1.594
Vertical Mover Mass	$M_v$	Kg	4.350

attached to two orthogonally mounted linear guides allowing for horizontal and vertical movement, is composed of a set of four type N35 permanent magnets (PM) attached to a ferromagnetic backing. The details of the hardware specifications are summarized in Table I.

The 3-phase AC current required to actuate the stator coils is provided by a set of three linear current amplifier modules (LCAM) which are sent commands via a PC. The horizontal and vertical position information is provided to the PC by two linear optical encoders with a resolution of 10  $\mu\text{m}$ . Controllers are implemented using the WINCON real-time code generator with Simulink as an interface.

The 2-DOF hardware has a horizontal range of approximately  $\pm 50$  mm and a vertical range of approximately  $\pm 10$  mm. The goal is to obtain steady-state set-point positioning accuracy of at least 0.1 mm and tracking accuracy approaching 0.1 mm over the above mentioned horizontal range and a vertical range of  $\pm 5$  mm, with as much speed as possible.

### III. MODEL OF 2-DOF SYSTEM

The following is a brief summary of the model derivation applied specifically to the 2-DOF system. The details of the modelling can be found in [3].

Consider the inertial frame of the single PMLSM that forms the basis of the 2-DOF system, which is shown in Figure 2. Let  $L_A$  be the depth of each PM along the  $z$  axis,  $h_m$  be the height of the magnets,  $p_m$  the number of PM's,  $g$  the air-gap length,  $t_1$  the slot pitch,  $b_0$  the slot aperture,  $\tau$  the PM pole pitch,  $\tau_p$  the PM pole arc,  $\mu_{rec}$  the relative PM recoil permeability, and  $\sigma_m$  the surface magnetic charge. To account for the effects of the stator slots, replace the air-gap  $g$  by the effective air-gap  $g_e$ , with  $g_e = gK_c$ , where  $K_c$  denotes Carter's coefficient. In addition, let  $i_a$ ,  $i_b$ , and  $i_c$  denote the instantaneous 3-phase currents applied to the PMLSM stator coils. Define  $W$  to be the number of turns of wire on each phase,  $p$  the number of pole pairs in the stator,  $\omega_c$  the coil pitch, and  $k_{w1}$  the winding factor.

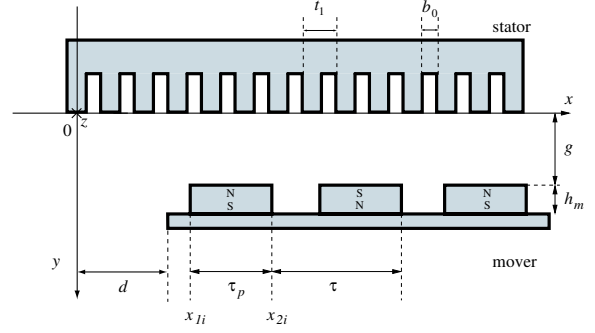


Fig. 2. Inertial frame of a single PMLSM

We define the horizontal motion to be along the  $x$ -axis while vertical motion is fixed to the  $y$ -axis. Defining  $G$  as the gravitational acceleration constant and  $M_h$  and  $M_v$  as the horizontal and vertical masses of the platform to be levitated<sup>1</sup>, one obtains the following 2-DOF system model

$$\begin{aligned} \dot{x}_1 &= x_2, \\ \dot{x}_2 &= G - L_4(x_1)[u_1^2 + u_2^2] + L_3(x_1)u_2 - L_2(x_1), \\ \dot{x}_3 &= x_4, \\ \dot{x}_4 &= -L_1(x_1)u_1, \end{aligned} \quad (1)$$

where

$$\begin{aligned} x &= [g, \dot{g}, d, \dot{d}]^T, \quad u = [i_q, i_d]^T, \\ L_1(x_1) &= \frac{K_1(x_1)}{M_h}, \\ L_i(x_1) &= \frac{K_i(x_1)}{M_v}, \quad i = 2, \dots, 4, \\ K_1(x_1) &= \frac{12\sqrt{2}Wk_{w1}p_mL_A\sigma_m\mu_0\tilde{\lambda}(x_1)\sinh(\frac{\pi}{\tau}h_m)\sin(\frac{\pi\tau_p}{2\tau})}{\pi pK_c(x_1)\sinh(\frac{\pi}{\tau}(h_m+x_1))}, \\ K_2(x_1) &= \frac{\tilde{\lambda}(x_1)L_A p_m \tau B_{pmy1}(x_1)^2}{4\mu_0}, \\ K_3(x_1) &= \frac{\tilde{\lambda}(x_1)3\sqrt{2}L_A p_m W k_{w1} B_{pmy1}(x_1) \coth(\frac{\pi}{\tau}(h_m+x_1))}{p^2 K_c(x_1)}, \\ K_4(x_1) &= \frac{\tilde{\lambda}(x_1)18L_A p_m W^2 k_{w1}^2 \mu_0 \coth^2(\frac{\pi}{\tau}(h_m+x_1))}{\tau p^2 K_c(x_1)^2}, \\ \tilde{\lambda}(x_1) &= 1 - \frac{b_0^2}{4t_1(x_1 + \frac{b_0}{2} + \frac{h_m}{\mu_{rec}})}. \end{aligned}$$

The function  $B_{pmy1}(x_1)$  represents the magnetic field produced by the PM's and is numerically approximated using a 12<sup>th</sup> degree polynomial. Furthermore,  $i_d$  and  $i_q$  represent the direct and quadrature current inputs to the PMLSM. They relate to the 3-phase currents as follows

$$\begin{aligned} i_d &= \frac{2}{3}\cos(\frac{\pi}{\tau}x_3)i_a + \frac{2}{3}\cos(\frac{\pi}{\tau}x_3 - \frac{2\pi}{3})i_b \\ &\quad + \frac{2}{3}\cos(\frac{\pi}{\tau}x_3 + \frac{2\pi}{3})i_c, \\ i_q &= -\frac{2}{3}\sin(\frac{\pi}{\tau}x_3)i_a - \frac{2}{3}\sin(\frac{\pi}{\tau}x_3 - \frac{2\pi}{3})i_b \\ &\quad - \frac{2}{3}\sin(\frac{\pi}{\tau}x_3 + \frac{2\pi}{3})i_c. \end{aligned} \quad (2)$$

The model (1) has unknown parameters and does not account for friction, cogging forces, and end effects. It was

<sup>1</sup>The horizontal and vertical masses of the platform are different due to the design of the 2-DOF apparatus

necessary in [4] to develop a system ID procedure and verify the model accuracy within a reasonable range of operation. These procedures are outlined in the section that follows.

#### IV. SYSTEM ID AND MODEL VERIFICATION

As discussed in [4], it was necessary to implement a system identification technique and apply it to the estimation of the unknown (or not perfectly known) model parameters from (1). The resulting system identification technique was based on the work presented by Pan and Başar in [5].

The results from [5] present a series of techniques to estimate constant parameters that enter linearly into nonlinear systems. The methods are based on minimization of a cost-to-come function and formulated in terms of a minimax design problem. While several variations of the estimation technique were presented, the one chosen for implementation was known as the reduced-order noise-perturbed full-state information (NPFISI) estimator. This technique was chosen in [4] because of its simplified structure and the fact that it did not require measurement of the state derivatives.

The reduced-order NPFISI estimator was used in three different ways. First, to estimate the horizontal dynamics. Second, to estimate a series of lumped parameters within the vertical dynamics. Lastly, to estimate all lumped parameters simultaneously within the horizontal and vertical dynamics.

In each case, it was necessary to have procedures in place to verify how accurately the predictions of the horizontal and vertical dynamics matched the actual behavior of the physical system. This was done by collecting a series of current and force measurements produced when the 2-DOF apparatus was actuated with a set of PID regulators.

The model verification results from [4] showed that the 2-DOF system model enhanced with estimated parameters could accurately predict the behavior of the physical system in an air-gap range between 15 and 25 mm and a horizontal range between  $-50$  mm and  $50$  mm. For air-gap values any smaller than the 15 mm limit, the effects of uncertainties such as the cogging force became significant and could no longer be ignored within the theoretical model.

To illustrate the effectiveness of the enhanced 2-DOF system model, Figures 3 and 4 compare the states measured from the actual system with the theoretical predictions.

Given that the plant is open-loop unstable, these results clearly demonstrate the accuracy of the final system model.

#### V. NONLINEAR CONTROLLER DESIGN

With the verification complete, the 2-DOF system model enhanced with estimated parameters can now be used to design a suitable nonlinear controller for actuation of the contactless positioning system.

In [3], two nonlinear stabilizers were presented, together with two procedures to rigorously estimate the range of operation of the associated closed-loop systems. Here we focus on the second controller presented in [3], which is based on feedback linearization, and implement a modification of it which addresses the presence of constant disturbances due to friction and bearing misalignment on

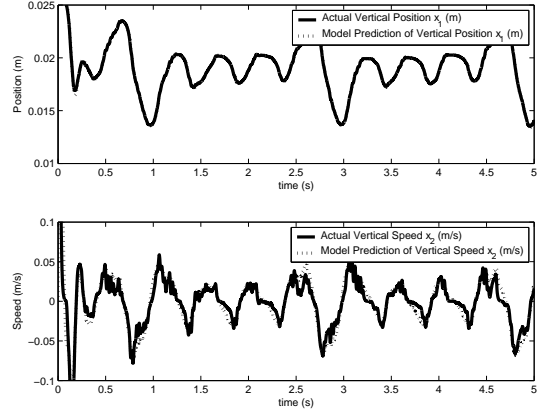


Fig. 3. Comparison between the actual and predicted vertical states

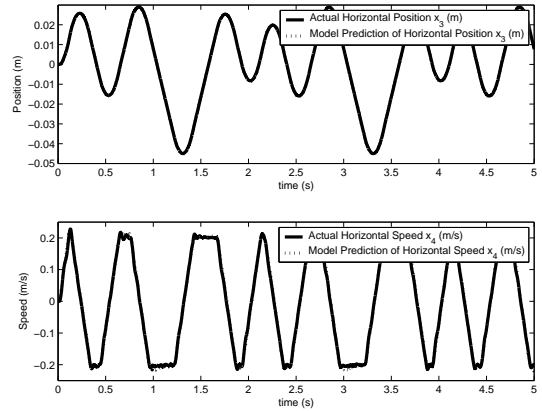


Fig. 4. Comparison between the actual and predicted horizontal states

the linear guides. Besides achieving set-point stabilization, we want the controller to also achieve sinusoidal tracking.

For convenience, we make a slight modification to the model (1), incorporating two parameters  $\Delta_1$  and  $\Delta_2$  representing constant uncertainties due to friction and bearing misalignment

$$\begin{aligned}\dot{x}_1 &= x_2, \\ \dot{x}_2 &= G - L_4(x_1)[u_1^2 + u_2^2] + L_3(x_1)u_2 \\ &\quad - L_2(x_1) + \Delta_2, \\ \dot{x}_3 &= x_4, \\ \dot{x}_4 &= -L_1(x_1)u_1 + \Delta_1.\end{aligned}$$

Consider next the feedback transformation

$$\begin{aligned}u_1 &= -\frac{v_1}{L_1(x_1)}, \\ u_2 &= \frac{L_3(x_1) - \sqrt{R(x_1, v_1, v_2)}}{2L_4(x_1)},\end{aligned}\tag{3}$$

where

$$\begin{aligned}R(x_1, v_1, v_2) &= L_3(x_1)^2 + 4L_4(x_1)(-v_2 \\ &\quad - L_4(x_1)U(x_1, v_1) - L_2(x_1) \\ &\quad + G), \\ U(x_1, v_1) &= \left(\frac{v_1}{L_1(x_1)}\right)^2.\end{aligned}$$

The resulting system reads as

$$\begin{aligned}\dot{x}_1 &= x_2, \\ \dot{x}_2 &= v_2 + \Delta_2, \\ \dot{x}_3 &= x_4, \\ \dot{x}_4 &= v_1 + \Delta_1.\end{aligned}\quad (4)$$

Note that the system has output  $y = (x_1, x_3)$ . Before proceeding further with the design of  $v_1$  and  $v_2$ , it is well to note that the feedback transformation (3) is well defined on the set  $\mathcal{A} = \{(x, v) : R(x_1, v_1, v_2) \geq 0, L_1(x_1) \neq 0, L_4(x_1) \neq 0\}$ . Thus, in order for our controller to make sense, after choosing  $v_1$  and  $v_2$  we need to estimate what is the range of operation of the device, that is, the largest set of feasible initial conditions  $x(0)$  guaranteeing that  $(x(t), v(t)) \in \mathcal{A}$  for all positive time. This is precisely what was done in Procedure 2 in [3]. Owing to the fact that the choice of  $v$  here is different than that in [3], Procedure 2 in [3] needs to be modified. Doing this is beyond the scope of this paper (and will be done elsewhere), so we rather focus on showing experimentally that our controller is well-defined over the range of interest.

We next choose  $v_1$  and  $v_2$  to make  $x_1$  and  $x_3$  track a constant step or a sinusoid of fixed frequency  $\omega_0$  (or a combination of the two) while rejecting the constant disturbances  $\Delta_1, \Delta_2$ . This control specification is best posed as a linear output regulation problem [6], [7], [8] where the exosystem is

$$\begin{aligned}\dot{w}_1 &= \omega_0 w_2, \\ \dot{w}_2 &= -\omega_0 w_1, \\ \dot{w}_3 &= \omega_0 w_4, \\ \dot{w}_4 &= -\omega_0 w_3, \\ \dot{w}_5 &= 0, \\ \dot{w}_6 &= 0, \\ \dot{w}_7 &= 0, \\ \dot{w}_8 &= 0, \\ (r_v, r_h, \Delta_1, \Delta_2) &= (w_1 + w_5, w_3 + w_6, w_7, w_8),\end{aligned}\quad (5)$$

and the output to be regulated is  $e = (e_1, e_2) = (x_1 - r_v, x_3 - r_h)$ . The internal model is made of two copies of the same system

$$\begin{aligned}\dot{\xi}_v &= \phi \xi_v + N e_1, & y_2 &= \Gamma \xi_v, \\ \dot{\xi}_h &= \phi \xi_h + N e_2, & y_1 &= \Gamma \xi_h,\end{aligned}\quad (6)$$

where

$$\phi = \begin{bmatrix} 0 & 1 & 0 \\ 0 & 0 & 1 \\ 0 & -\omega_0^2 & 0 \end{bmatrix}, \quad N = \begin{bmatrix} 0 \\ 0 \\ 1 \end{bmatrix}, \quad \Gamma = [1 \ 0 \ 0].$$

It is useful to think of the  $\xi_v$  and  $\xi_h$  subsystems in (6) as being two internal models for the vertical and horizontal dynamics, respectively. For simplicity of implementation, we exploit the fact that  $w_1, \dots, w_4$  in the exosystem (5) and  $x_1, \dots, x_4$  in (4) can be assumed to be available for feedback

and complete the output regulator design by letting

$$v_1 = K_h \begin{bmatrix} e_2 \\ \dot{e}_2 \\ \xi_h \end{bmatrix} + \Gamma \xi_h, \quad v_2 = K_v \begin{bmatrix} e_1 \\ \dot{e}_1 \\ \xi_v \end{bmatrix} + \Gamma \xi_v, \quad (7)$$

where  $K_h$  and  $K_v$  are chosen so as to stabilize the augmented system below when  $\Delta_1 = \Delta_2 = r_v = r_h = 0$ .

$$\begin{aligned}\dot{x}_1 &= x_2, \\ \dot{x}_2 &= K_v \begin{bmatrix} x_1 \\ x_2 \\ \xi_v \end{bmatrix} + \Gamma \xi_v, \\ \dot{x}_3 &= x_4, \\ \dot{x}_4 &= K_h \begin{bmatrix} x_3 \\ x_4 \\ \xi_h \end{bmatrix} + \Gamma \xi_h, \\ \dot{\xi}_v &= \phi \xi_v + N x_1, \\ \dot{\xi}_h &= \phi \xi_h + N x_3.\end{aligned}$$

The final controller is thus given by (3), (6), and (7). In what follows, the controller performance is evaluated.

## VI. EXPERIMENTAL RESULTS

The resulting nonlinear controller was implemented using WINCON. Its ability to track step and sinusoidal responses was evaluated and compared with some linear counterparts.

### A. Controller Set-Point Performance

Using the following values for the horizontal and vertical controller gains in (7),

$$\begin{aligned}K_h &= [ -1182 \quad -55 \quad -154440 \quad -45128 \quad -11924 ], \\ K_v &= [ -1662 \quad -65 \quad -360360 \quad -103350 \quad -20332 ],\end{aligned}$$

the resulting nonlinear controller was used to stabilize the system to a series of set-points over the ranges of  $[-50 \text{ mm}, 50 \text{ mm}]$  horizontal and  $[15 \text{ mm}, 25 \text{ mm}]$  vertical. Figure 5 shows the response of the vertical system states to the step commands in addition to the absolute vertical positioning accuracy. Figure 6 displays the same results for the horizontal system states. Finally, Figure 7 demonstrates the amount of current input required to achieve these results.

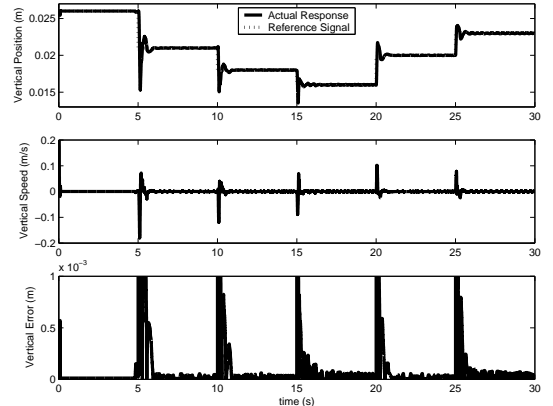


Fig. 5. Plots of vertical state responses to set-point commands

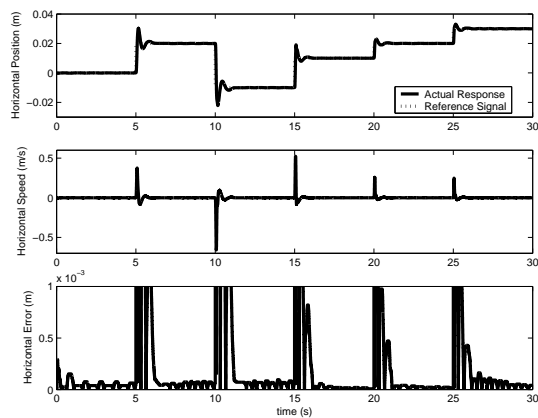


Fig. 6. Plots of horizontal state responses to set-point commands

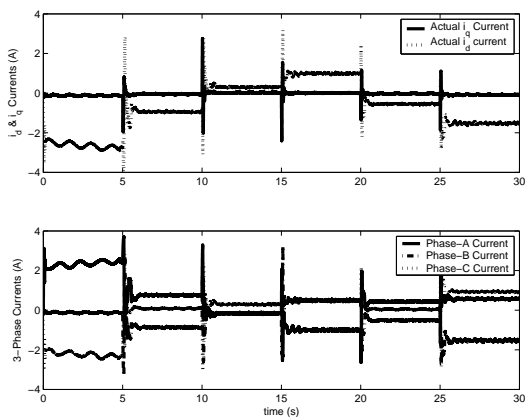


Fig. 7. Plots of current inputs required for set-point commands

The plots demonstrate the effectiveness of the nonlinear controller in performing set-point stabilization to the required 0.1 mm accuracy with settling time below 3 s over a wide operating range. Different experiments, not reported here, showed that the controller was capable of driving the tracking error to within encoder resolution (10  $\mu\text{m}$ ) in about 10 s.

Although no additional controller specifications were set, it should be noted that while the present controller gains produce short transient, the overshoot on the vertical steps is quite large and could potentially limit the range of motion. By making the following adjustment to the vertical controller gains,

$$K_v = [ -1592 \quad -81 \quad -55736 \quad -11573 \quad -15825 ],$$

Figure 8 shows how the step response now exhibits much smaller vertical overshoot at the cost of a longer settling time (still below 3 s). Depending on the final industrial application, either the overshoot or settling time may be a more important factor. The results show that controller adjustments can be made to accommodate either requirement.

The superior performance of the nonlinear controller is clearly visible when compared with a linear counterpart. The linear controller under consideration for this comparison is the same linear output regulator from (7), but without the addition of the feedback transformation (3). In order

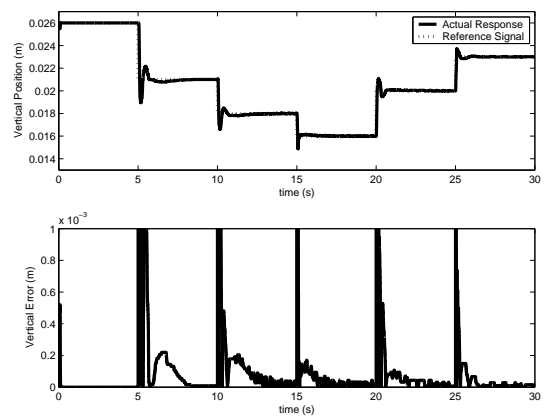


Fig. 8. Plots of vertical step response when controller gains are adjusted

to make a fair comparison, the model in (1) is linearized around a set-point  $\bar{x}$  and an output regulator with the same structure as (6)-(7) is designed so that the resulting closed-loop system poles coincide with the poles that the nonlinear controller induces in the feedback linearized plant. Next, various step responses are measured with steps of varying magnitude, ending at  $\bar{x}$ . Figure 9 shows the results. The first step response is small, starting from the initial condition of (0.026 m, 0, 0, 0) and ending at  $\bar{x} = (0.024 \text{ m}, 0, 0.005 \text{ m}, 0)$ . The second step response is larger, starting at the same initial condition as before but terminating at  $\bar{x} = (0.018 \text{ m}, 0, 0.020 \text{ m}, 0)$ .

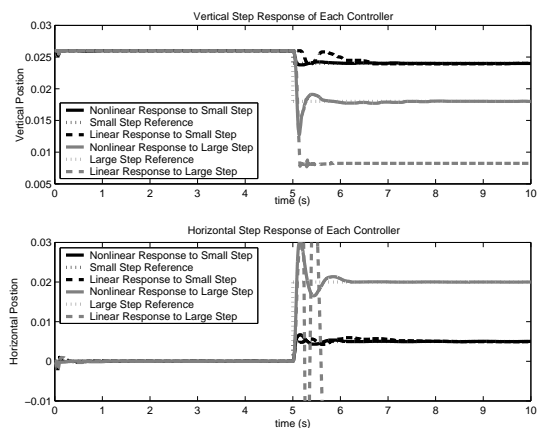


Fig. 9. Plots comparing linear and nonlinear controller performance

The results show that while both the linear and nonlinear controller can handle a small step command, the linear response demonstrates a much larger transience and settling time. When subjected to the larger step command, the linear controller makes the plant unstable while the nonlinear controller still exhibits excellent performance. It should be noted that around 5.5 seconds, the instability exhibited by the linear controller causes a safety mechanism within the real-time code to shut-down the system, which is why the oscillations halt at that point in time within Figure 9. An equivalent comparison was attempted between the nonlinear controller and the PID controller that was implemented to generate

the necessary persistency of excitation for the system ID procedure. However, since the PID performed very poorly, it was clear that a detailed comparison was not necessary.

### B. Controller Tracking Performance

For the tracking experiments, we choose  $r_h(t)$  and  $r_v(t)$  to be sinusoidal signals with amplitude 30 mm and 5 mm, respectively, and a frequency of  $\omega_0 = 1.5\pi$  rad/sec. The vertical reference  $r_v(t)$  also includes an offset of 20 mm. The same controller gains from the set-point experiments were employed in the nonlinear controller. Figure 10 summarizes the tracking results obtained from the nonlinear controller. The horizontal tracking error averages about 0.11 mm with occasional peaks that reach 0.4 mm. The vertical tracking error meanwhile averages 0.24 mm with peaks that reach 0.8 mm

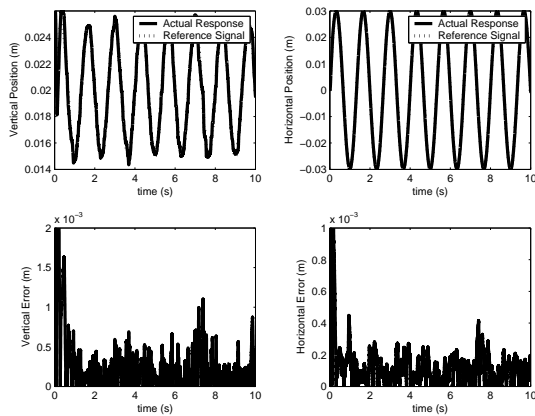


Fig. 10. Plots showing tracking performance of nonlinear controller.

The nonlinear tracking performance was deemed satisfactory despite the fact that the vertical error is about twice the desired specification. While adjustments to the tracking performance were attempted, no significant improvements were achieved beyond the results that were presented. This is likely due to hardware limitations, namely the Coulumb friction of the linear guides and their imperfect alignment. The tracking performance of the nonlinear controller is significantly better than that of a basic PID arrangement that was utilized during the model verification experiments in [4]. Figure 11 summarizes the tracking results obtained when the PID-based controller is used to track the same sinusoidal references as in the nonlinear case.

It can clearly be seen that the PID-based controller produces significantly more tracking error. Specifically, the average horizontal error is now about 0.19 mm, while the vertical error now approaches 0.9 mm. The nonlinear controller has therefore been shown to produce an improvement of at least 50% in the tracking error when compared to the PID arrangement.

## VII. CONCLUSIONS AND FUTURE WORK

This paper has shown how a system model enhanced using estimated parameters from [4] was used to design

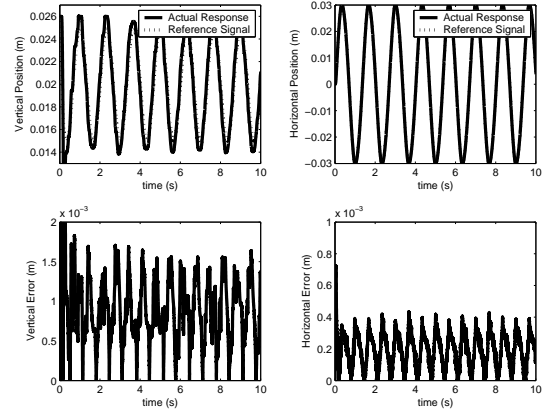


Fig. 11. Plots showing tracking performance of PID-based controller

a nonlinear controller, based on feedback linearization and output regulation, to actuate a 2-DOF positioning system employing a single PMLSM and constructed by Quanser Inc. The experimental results obtained from implementing the nonlinear controller demonstrate that the positioning system is capable of satisfactory set-point and sinusoidal tracking with a performance that exceeded some linear counterparts.

These results show promise for the next phase of the research, which entails implementing a more sophisticated next-generation positioning system, with 3-DOF and constructed from 4 PMLSM's. Once the 3-DOF apparatus is complete, the nonlinear controller design procedure presented in this article will be implemented on this new test platform with more rigid control specifications.

Future work will extend the concept beyond the 3-DOF implementation, increasing the number of degrees-of-freedom, decreasing the dependence on linear guides and bearings, and eventually produce a contactless prototype more suitable for industrial applications.

## REFERENCES

- [1] K.-Y. Tsai and J.-Y. Yen, "Servo system design of a high-resolution piezo-driven fine stage for step-and-repeat microlithography systems," in *The 25th Annual Conference of the IEEE Industrial Electronics Society*, vol. 1, 1999, pp. 11–16.
- [2] W. Kim and D. Trumper, "High-precision levitation stage for photolithography," *Precision Engineering*, vol. 22, pp. 66–67, 1998.
- [3] M. Maggiore and R. Becerril, "Modeling and control design for a magnetic levitation system," *International Journal of Control*, vol. 77, no. 10, pp. 964–977, 2004.
- [4] R. Owen and M. Maggiore, "Implementation and model verification of a magnetic levitation system," to appear in the *Proceedings of the American Control Conference*, 2005.
- [5] G. Didinsky, Z. Pan, and T. Basar, "Parameter identification for uncertain plants using  $\mathcal{H}^\infty$  methods," *Automatica*, vol. 31, no. 9, pp. 1227–1250, 1995.
- [6] E. J. Davison, "The robust control of a servomechanism problem for linear time-invariant multivariable systems," *IEEE Transactions on Automatic Control*, vol. 21, pp. 25–34, 1976.
- [7] B. A. Francis and W. M. Wonham, "The internal model principle of control theory," *Automatica*, vol. 12, pp. 457–465, 1976.
- [8] B. A. Francis, "The linear multivariable regulator problem," *SIAM Journal on Control and Optimization*, vol. 14, pp. 486–505, 1977.